

Microscopic approach to the bcc phase of solid ^4He

R. Rota and J. Boronat*

*Departament de Física i Enginyeria Nuclear, Campus Nord B4-B5,
Universitat Politècnica de Catalunya, E-08034 Barcelona, Spain*

Abstract

The coexistence between the hcp and bcc phases of solid ^4He at fixed pressure, and at three different temperatures, is studied by means of the path integral Monte Carlo method. Microscopic results for the main energetic and structure properties of the two phases are reported. The differences between hcp and bcc ^4He are shown to be small with the obvious exception of the static structure factor. When crossing the phase transition line, the most significant changes are observed in the kinetic energy per particle and in the Lindemann ratio, both pointing to a less correlated quantum solid in the bcc side. No off-diagonal long-range order is observed in the the hcp and bcc perfect lattices.

Keywords: solid ^4He ; bcc phase; quantum Monte Carlo

PACS numbers: 67.80.B-, 02.70.Ss

I. INTRODUCTION

Quantum solids have been studied for many years in the context of low-temperature condensed-matter physics. Contrarily to classical solids, the high zero-point motion of the atoms makes their oscillations around the lattice sites significant even at very low temperature. This makes quantum crystals have large Lindemann ratios and unambiguous anharmonic effects. Solid helium in its two stable isotopes ^4He and ^3He , and their mixtures, represent the best example of quantum solids [1]. Helium has a mass so small and its atomic interaction is so shallow that remains liquid even in the limit of zero temperature. It is necessary to pressurize ^4He and ^3He up to ~ 25 and 30 bar, respectively, to freeze them at $T = 0$. Because of the different mass and its different quantum statistics (^4He is a boson and ^3He is a fermion), the solidification is in the two cases different: ^4He crystallizes into an hcp solid whereas ^3He does it into a bcc one. The phase diagram of both systems offers also the counterpart: ^3He evolves to an hcp phase at higher pressures and ^4He presents a very narrow bcc region at temperatures $T \sim 1.5 - 1.7$ K.

The theoretical and experimental interest on solid ^4He has been reinforced since the experimental observation in 2004 of non conventional rotation of inertia (NCRI) in torsional oscillator experiments by Kim and Chan [2]. This experiment, subsequent ones by the same team, and independent measures in a number of different laboratories have confirmed these findings but the fraction of mass decoupled (superfluid fraction) depends strongly on the quality of the crystal [3]. The experimental data and their interpretation as unambiguous signatures of the existence of the supersolid state are still matter of debate. The observation by Beamish and collaborators [4] of an increase of the shear modulus of hcp ^4He at nearly the same onset temperature for NCRI ($T_0 \simeq 100$ mK) has lead to think that, at least in a partial way, the NCRI signal can be attributed to the change in the elastic properties. However, there is a general consensus that not all the torsional oscillator results can be interpreted solely on plasticity terms [5, 6].

The main focus of this recent research activity has been hcp ^4He since this is the stable phase at very low temperatures. However, Eyal et al.[7] have reported recently torsional oscillator experiments on bcc ^4He at temperatures between 1.3 and 1.9 K that show similar phenomena to those measured in the hcp phase below 100 mK. This is a surprising result since, even if the disorder of the sample is eventually large, the temperatures of this experiment are an order of magnitude larger than in hcp. This is not the only relevant result related to the bcc phase that emerged in the last years. Some time ago, Markovich et al.[8] reported neutron-scattering measurements of phonons in bcc ^4He and found an unexpected “opticlike” mode along the $[110]$ direction. This new mode has been theoretically interpreted by Gov [9] in terms of correlated dipolar interactions.

The boundaries of the bcc phase of ^4He were first determined by Vignos and Fairbank [10] in 1961 after analyzing their measurements of the velocity of longitudinal sound. The existence of this phase was confirmed after x-ray scattering by Schuch and Mills [11]. Later on, Grilly and Mills [12] measured the volume change along the hcp-bcc coexistence line and Edwards and Pandorf [13] performed accurate measurements of the heat capacity. Updated accounts of the thermodynamic properties of bcc ^4He can be found in Refs. [14, 15]. In Fig. 1, the P - T phase diagram in the region of interest is plotted. As one can see, the stability of the bcc solid is only ~ 0.04 K wide at fixed pressure and it represents an intermediate phase between the hcp solid and the superfluid in the range of temperatures $T \simeq 1.5$ - 1.75 K.

From the theoretical point of view, the high anharmonicity of solid ^4He makes its analysis much more demanding since the usual harmonic theory used in classical solids is not applicable. The self-consistent phonon (SCP) theory incorporates approximately the short-range correlations induced by the interatomic potential, leading to reasonable descriptions of many of its properties [1]. However, a more accurate study of quantum solids requires of a microscopic approach. To this end, quantum Monte Carlo (QMC) methods have been widely applied in the past to the study of solid ^4He . However, the main part of the QMC work is devoted to the hcp phase since it is the stable crystal in the limit of very low temperature. Results on the bcc phase are scarce and concentrated to the limit of zero temperature [16–18]. To our knowledge, the only existing work in the bcc stable P - T region shown in Fig. 1 was done by Ceperley [19] with the main goal of

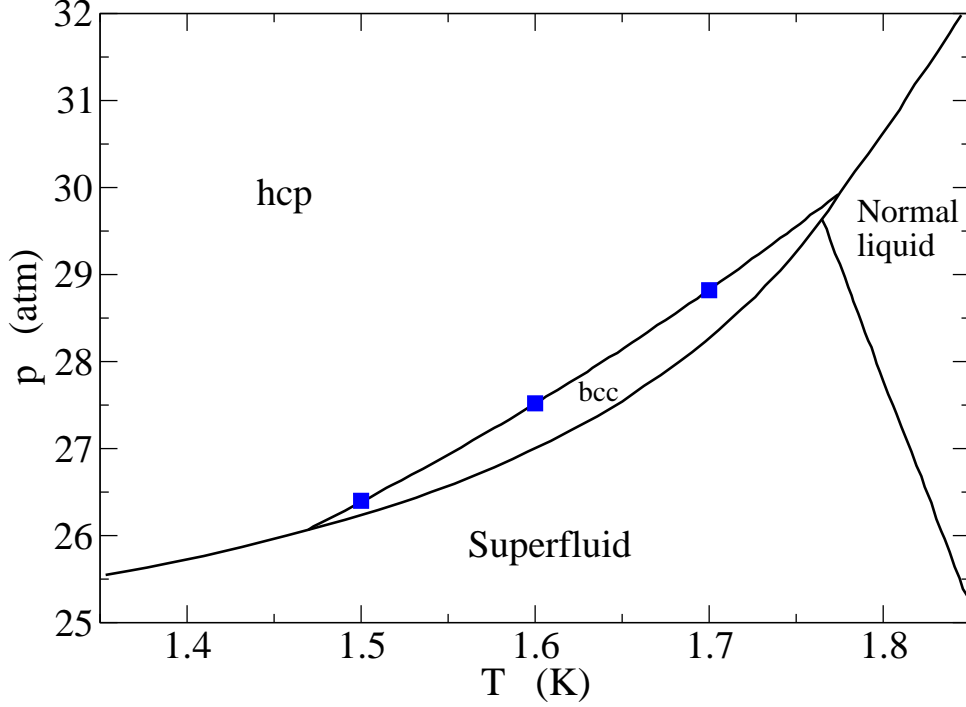


FIG. 1: (Color online) Pressure-temperature phase diagram in the stable region of the bcc phase of solid ^4He . The squares correspond to the thermodynamic points studied in the present work.

estimating the momentum distribution and kinetic energies after some neutron scattering experiments [20]. Our aim in the present work is to carry out a QMC study of the bcc phase at three temperatures and densities corresponding to the experimental points shown in Fig. 1 and compare them with the corresponding hcp ones along the coexistence line. As we will show, the differences between both phases is found small except for the kinetic energies and Lindemann ratios where the less correlated character of the bcc lattice is revealed.

The rest of the paper is organized as follows. In Sec. II, we introduce the path integral Monte Carlo (PIMC) method used in our simulations. Sec. III comprises the main results obtained, and finally a brief account of the main conclusions is contained in Sec. IV.

II. THEORETICAL APPROACH

The structure and energetic properties of the hcp-bcc coexistence line have been studied using the path integral Monte Carlo (PIMC) method. PIMC provides a fundamental approach in the study of strongly interacting quantum systems at finite temperature by means of an stochastic estimation of the thermal density matrix [21]. As it is well known, the partition function

$$Z = \text{Tr}(e^{-\beta\hat{H}}) = \int d\mathbf{R} \langle \mathbf{R} | e^{-\beta\hat{H}} | \mathbf{R} \rangle \quad (1)$$

allows for a full microscopic description of the properties of a given system with Hamiltonian $\hat{H} = \hat{K} + \hat{V}$ at a temperature $T = (k_B\beta)^{-1}$ (we use the position basis $|R\rangle = |\mathbf{r}_1, \dots, \mathbf{r}_N\rangle$, with N the number of particles). However, in quantum systems the noncommutativity of the kinetic and potential energy operators (respectively, \hat{K} and \hat{V}) makes impractical a direct calculation of Z using its definition (1).

The basic idea of PIMC is to use the convolution property of the thermal density matrix $\rho(R, R'; \beta) = \langle R | e^{-\beta\hat{H}} | R' \rangle$, in order to rewrite the partition function as

$$Z = \int \prod_{i=0}^{M-1} dR_i \rho(R_i, R_{i+1}; \varepsilon), \quad (2)$$

with $\varepsilon = \beta/M$ and the boundary condition $R_M = R_0$. For sufficiently large M , we recover the high-temperature limit of the thermal density matrix, where it is legitimate to separate the kinetic contribution from the potential one (Primitive Approximation). If one ignores the quantum statistics of particles, the distribution law appearing in Eq. 2 is positive definite and can be interpreted as a probability distribution function which can be sampled by standard metropolis Monte Carlo methods.

In practice, the PIMC method consists in mapping the finite-temperature quantum system to a classical system made up of closed ring polymers. This technique may be referred as an “exact” method, in the sense that using an accurate approximation for the high-temperature density matrices, the results are not affected by this approximation within the statistical error. However, the number M of convolution terms (beads) necessary to reach the convergence of Eq. 2 to the exact value of Z is inversely proportional to the temperature of the system. This means that, when approaching the interesting quantum regime at very low temperature, M increases fast making simulations hard, if not impossible, due to the very low efficiency in the sampling of the long chains involved. To overcome this problem, it is important to work out high-order approximation schemes for the density matrix, able to work with larger values of ε . The approximation we use in this work is called Chin Approximation (CA) [22]. CA is based on a fourth-order expansion of the operator $e^{-\beta\hat{H}}$ which makes use of the double commutator $[[\hat{V}, \hat{K}], \hat{V}]$, this term being related to the gradient of the interatomic potential. With respect to the Takahashi-Imada approximation [23], which is accurate to fourth order only for the trace, the new feature appearing in the CA is the presence of coefficients weighting the different terms in the expansion of the action. These coefficients are continuously tunable, making possible to force the error terms of fourth order to roughly cancel each other and get an effective sixth-order approximation.

An additional problem one has to deal with when simulating quantum many-body systems with PIMC arises from the indistinguishable nature of particles. In the case of bosons like ^4He , the indistinguishability of particles does not change the positivity of the probability distribution in Eq. 2 and the symmetry of $\rho(R, R'; \beta)$ can be recovered via the direct sampling of permutations between the ring polymers representing the quantum particles. To this purpose, we use the Worm Algorithm (WA) [24] which samples very efficiently the permutation space. The basic idea of this technique is to work in an extended configuration space, given by the union of the ensemble Z , formed by the usual closed-ring configurations, and the ensemble G , which is made up of configurations where all the polymers but one are closed. Thanks to the presence of an open polymer, one can search the atoms involved in a permutation cycle by means of single particle updates, which do not suffer of a low acceptance rate and guarantee an efficient and ergodic sampling of the bosonic permutations. We have to notice that the probability distribution used to sample the configurations in G is not equal to the one appearing in Eq. 2 and, therefore, these configurations cannot be used to calculate diagonal properties, such as the energy or the superfluid density. However, the G -configurations can be used to compute off-diagonal observables such as the one-body density matrix $\rho_1(\mathbf{r}_1, \mathbf{r}'_1)$. Furthermore, the WA samples both diagonal and off-diagonal configurations and then it is able to give an estimation of the normalization factor of $\rho_1(\mathbf{r}_1, \mathbf{r}'_1)$. In this way, one can compute the properly normalized one-body density matrix and so to avoid the systematic uncertainties introduced by an a posteriori normalization factor.

TABLE I: PIMC results of the total (E/N) and partial energies (V/N , K/N) for the three thermodynamic points in the hcp-bcc coexistence line here analyzed. Experimental values of the bcc energies, reported in the first row, are taken from Ref. [14]. Figures in parenthesis stand for the statistical errors.

	A ($T = 1.5$ K)		B ($T = 1.6$ K)		C ($T = 1.7$ K)	
	bcc	hcp	bcc	hcp	bcc	hcp
E/N expt. (K)	-5.95		-5.93		-5.91	
E/N PIMC (K)	-6.166(7)	-6.058(7)	-6.137(8)	-6.025(7)	-6.091(9)	-5.984(6)
V/N (K)	-30.103(3)	-30.448(3)	-30.230(3)	-30.605(3)	-30.372(3)	-30.752(2)
K/N (K)	23.936(5)	24.391(7)	24.093(5)	24.580(5)	24.281(7)	24.768(5)

III. RESULTS

We have carried out our PIMC study of the hcp-bcc coexistence line particularizing the simulations in the three experimental thermodynamic points shown in Fig. 1. Explicitly, in the P - T phase diagram the coordinates of these points are A = (1.5, 26.419), B = (1.6, 27.572), and C = (1.7, 29.029) with units of bar and kelvin for the pressure and temperature, respectively. The corresponding densities are taken from the experimental data contained in Refs. [14, 15]: ($\rho_A^{\text{hcp}} = 0.028834$, $\rho_A^{\text{bcc}} = 0.028571$), ($\rho_B^{\text{hcp}} = 0.028954$, $\rho_B^{\text{bcc}} = 0.028679$), and ($\rho_C^{\text{hcp}} = 0.029080$, $\rho_C^{\text{bcc}} = 0.028805$), all in units of \AA^{-3} .

In the Hamiltonian of the system the potential part is built as a sum of pair-wise interatomic potentials, $\hat{V} = \sum_{i<j}^N V(r_{ij})$, with $V(r)$ of Aziz type [25]. Simulations are performed using periodic boundary conditions with a number of atoms per simulation cell of $N = 180$ (hcp) and $N = 128$ (bcc); tail corrections to the energy due to the use of a finite number of particles are estimated by running simulations with different N values and extrapolating its linear behavior in $1/N$ to the thermodynamic limit $1/N \rightarrow 0$ [26]. The convergence to the limit $\varepsilon \rightarrow 0$ is achieved with relatively large values of ε ($\varepsilon = 0.010 \text{ K}^{-1}$) due to the high accuracy of the CA [22].

PIMC results for the total energy per particle in the three mentioned thermodynamic points are reported in Table 1. The difference between the energies of the two lattices in the coexistence line is small but, in the three cases, the bcc energies are larger than the hcp ones (in absolute values). This difference is mainly due to the slightly smaller density in the bcc side with respect to the hcp one, with a smaller effect of the lattice type (at the same density). On the other hand, PIMC energies lie below the available experimental energies of the bcc solid in an amount ~ 0.20 K, a feature already observed in liquid ^4He and attributable to the particular Aziz potential used in the present simulations [27].

In Table 1, we also have included the partial energies per particle. The results for the kinetic energy per particle K/N are the most relevant because it is possible to measure them using deep inelastic neutron scattering. As it is well known, if the momentum of the incoming neutron is high enough the impulse approximation holds and the atomic momentum distribution $n(k)$ is attainable, and from it the kinetic energy. Blasdel et al.[20] reported experimental results of K/N for both solid lattices: at $T = 1.07$ K and hcp $K/N = 23.6$ K, and at $T = 1.72$ and bcc $K/N = 23.7$ K (the densities of both phases were the same). If just the classical estimation $3/2kT$ is considered for an isothermical comparison, one can see that the kinetic energy of the bcc crystal is significantly smaller. PIMC results by Ceperley [19] also agrees with this trend (in this case the comparison is made between fcc and bcc lattices). Our present results allow for a best comparison since they are obtained following the coexistence line. As one can see in Table 1, there is a nearly constant decrease of ~ 0.5 K when going from the hcp point to the bcc one and our results are in overall agreement with the experimental determinations of Blasdel et al.[20]. The thermal effects in the kinetic energy for any of the two lattices are dominated by the classical term $3/2kT$ that gives a difference

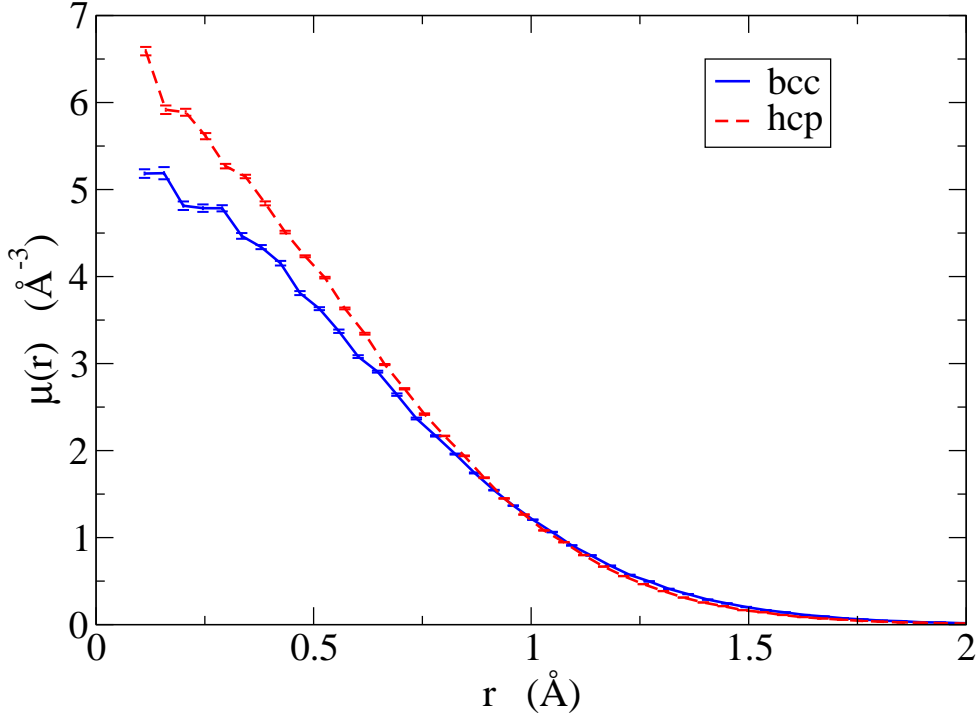


FIG. 2: (Color online) Density profile $\mu(r)$ of ^4He atoms around the lattice sites for the two lattices at $T = 1.5$ K.

of 0.15 K from one point to the next one.

We have also calculated some structural properties of the bcc phase to better characterize it and to identify specific signatures of this lattice symmetry. One of the most relevant in the microscopic study of any solid phase is the density profile $\mu(r)$, defined as the probability of finding a particle in the interval $(r, r + dr)$ around any of the lattice points of the crystal. Results of $\mu(r)$ at the thermodynamic point A and for the two coexistence lattices are shown in Fig. 2. As expected, the density profile of the bcc crystal is a bit wider than the hcp one, with a decrease of localization as corresponds to its slightly more open structure. From the density profile it is possible to calculate the mean squared displacement around a site,

$$\langle \mathbf{u} \rangle^2 = 4\pi \int_0^\infty dr r^4 \mu(r), \quad (3)$$

and from it to estimate the Lindemann ratio,

$$\gamma = \frac{\sqrt{\langle \mathbf{u} \rangle^2}}{a}, \quad (4)$$

a being the nearest-neighbor distance in the perfect crystalline lattice. We have obtained $\gamma_{\text{hcp}} = 0.26$ and $\gamma_{\text{bcc}} = 0.28$, in agreement with experimental data [1]. The Lindemann ratio is a good measure of the zero-point motion and thus the larger value of γ for the bcc lattice points to an enhancement of its quantum nature.

In Fig. 3, we show results of the two-body radial distribution function for both lattices in the coexistence at $T = 1.5$ K. One can see the usual oscillations due to the periodic spatial order and only a tiny difference

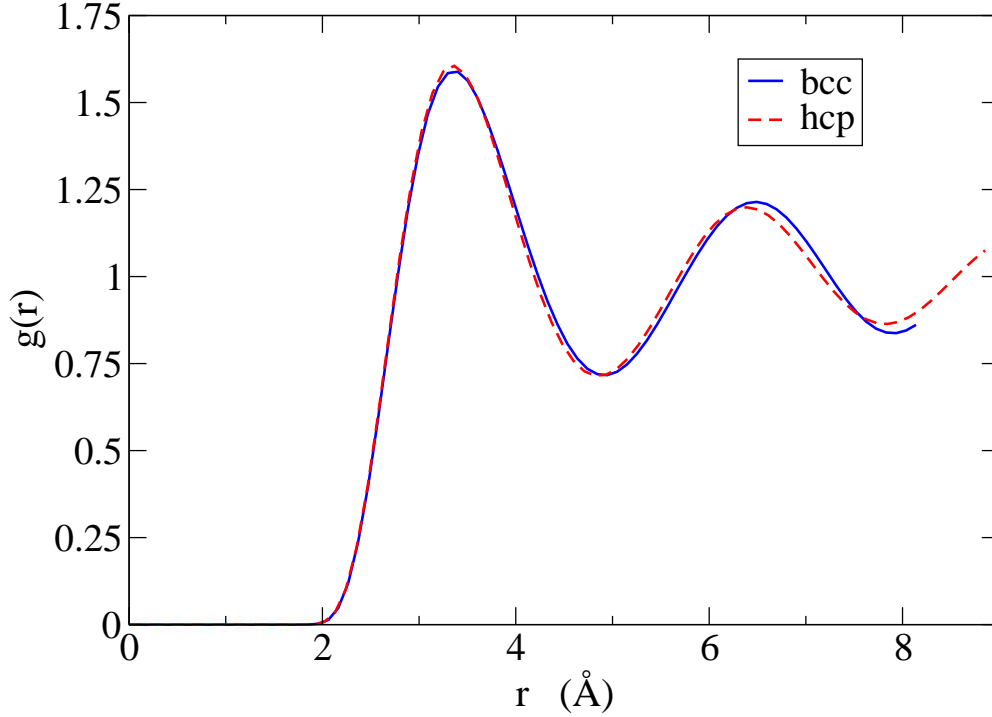


FIG. 3: (Color online) Two-body radial distribution function for the hcp and bcc phases of solid ^4He at $T = 1.5$ K.

between both lattices. The height of the main peak of the bcc $g(r)$ is slightly smaller than the hcp one but this is more an effect of its smaller density than a consequence of the lattice symmetry. The difference in the spatial order induced by the lattice is more clear in reciprocal space by defining the static structure factor

$$S(q) = \frac{1}{N} \left\langle \sum_{i=1}^N e^{-i\mathbf{q}\cdot\mathbf{r}_i} \sum_{j=1}^N e^{i\mathbf{q}\cdot\mathbf{r}_j} \right\rangle. \quad (5)$$

Results for $S(q)$ at both sides of the coexistence line at $T = 1.5$ K are shown in Fig. 4. Several Bragg peaks are clearly identified; they are located at the expected points for each type of lattice. As is well known from solid state physics, the determination of the static structure factor is the best way for identifying the particular lattice of the crystal and, in fact, the x-ray measures by Schuch and Mills [11] were the definite prove of the existence of a stability region for bcc ^4He .

Much of our present interest on the bcc phase of solid ^4He lies on the unexpected results found by Eyal et al.[7] which point to disorder-induced mobility, that manifests in the TO experiments as the typical mass decoupling observed in hcp at very low temperatures ($T < 200$ mK). This could open the possibility of a supersolid scenario at higher temperatures. Any signature of supersolidity would appear in off-diagonal properties of the system, like the one-body density matrix $\rho_1(r)$ defined as

$$\frac{\rho_1(\mathbf{r}_1, \mathbf{r}'_1)}{\rho} = \frac{1}{Z} \int d\mathbf{r}_2, \dots, \mathbf{r}_N \rho(\mathbf{r}_1, \dots, \mathbf{r}_N; \mathbf{r}'_1, \dots, \mathbf{r}_N; \beta). \quad (6)$$

With the help of the WA one can calculate this function with high efficiency and avoid normalization problems that were present in other permutation sampling methods. In Fig. 5, we show results for $\rho_1(r)$ at

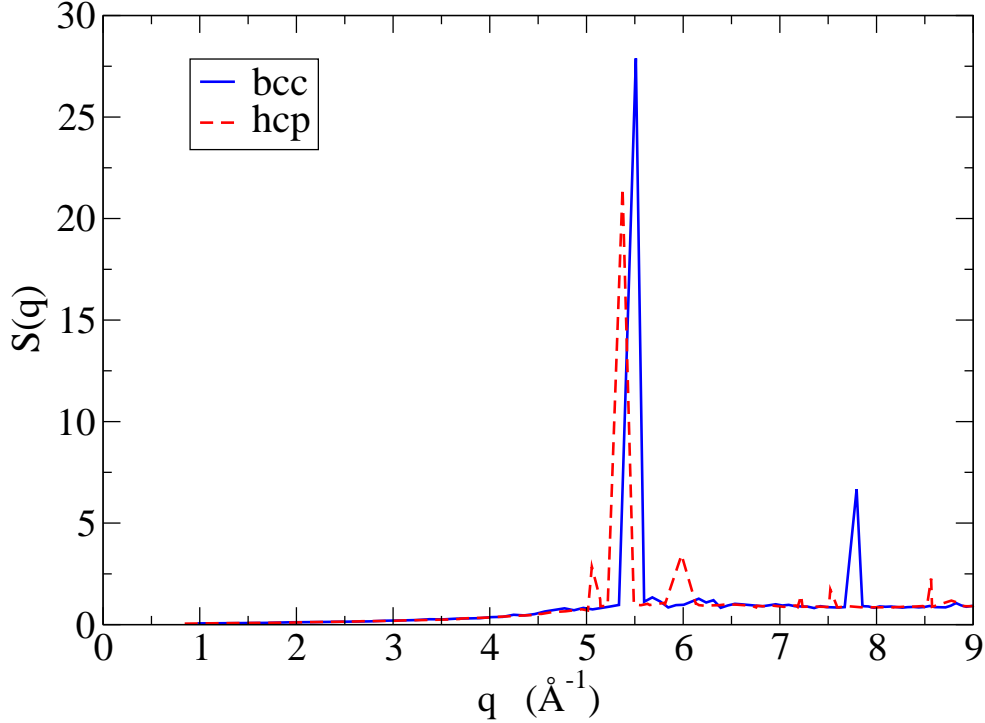


FIG. 4: (Color online) Static structure factor for the hcp and bcc phases of solid ^4He at $T = 1.5$ K.

$T = 1.5$ K calculated for the two lattices. The shape of the two results is very similar and coincides with previous estimations: a fast decay up to ~ 4 Å, a small increase near the position of the first neighbor, and finally a kind of exponential decay to zero. The most relevant feature of these results is the absence of off-diagonal long-range order, which would manifest as a nonzero asymptotic constant (condensate fraction) when $r \rightarrow \infty$. Therefore, neither the perfect hcp crystal nor the perfect bcc one show signals of supersolidity according to our PIMC results.

IV. CONCLUSIONS

We have performed a microscopic study of the coexistence hcp-bcc line in solid ^4He using the path integral Monte Carlo method. This method allows for a nearly ab-initio study where the only inputs are the mass and the interatomic potentials. Our goal has been to get an accurate view of the possible differences between both lattices along the measured coexistence line. Apart from the intrinsic interest on the study of the bcc phase, which has been scarcely studied in the past, we were stimulated by the recent activity of Polturak and collaborators [7] who have shown intriguing results using the TO technique.

Our results show a small influence of the lattice type when crossing the coexistence line. The internal energies are similar and the differences between both crystals are more attributable to the slight difference in density than to the particular crystal symmetry. Also the radial distribution functions show only very tiny differences. What is more significant is the drop in the kinetic energy from the hcp phase to the bcc one, that we have estimated to be 0.5 K, and that is in overall agreement with experimental findings

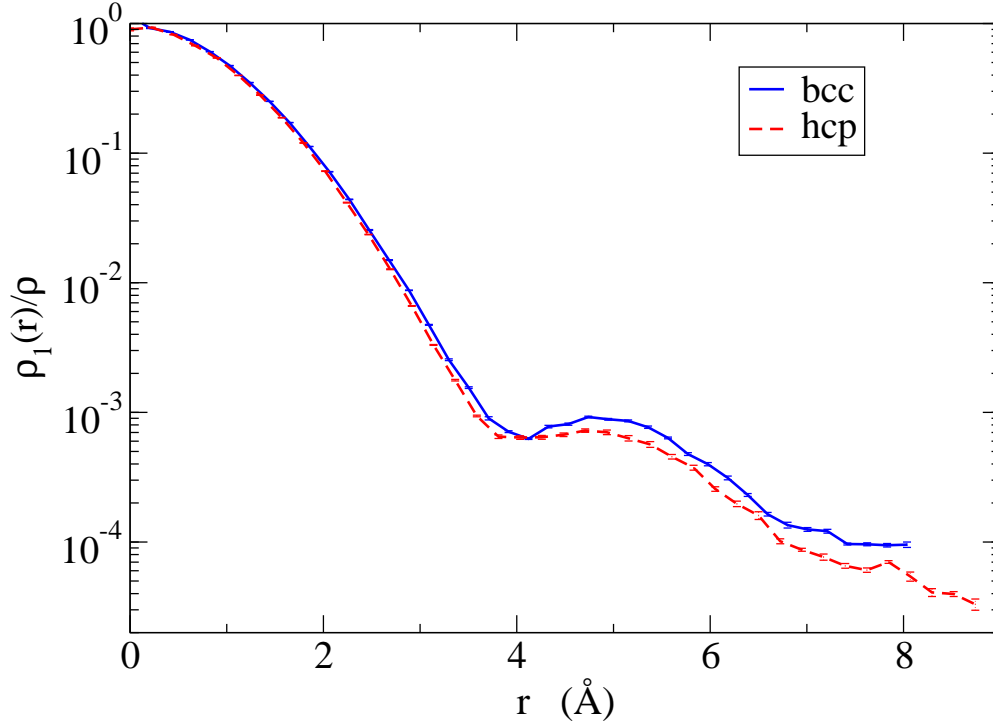


FIG. 5: (Color online) One-body density matrix for the hcp and bcc phases of solid ^4He at $T = 1.5$ K.

[20]. The less compact structure of the bcc solid is also observed in the results obtained for the density profiles and the Lindemann ratios. Finally, we have calculated the one-body density matrix in both sides of the coexistence line without observing any relevant difference between them and, more importantly, without obtaining off-diagonal long-range order which allows us to conclude that a perfect bcc crystal, at the temperatures where this phase is stable, is not a supersolid. Work is in progress in our group to determine if the introduction of point defects (vacancies) in the bcc crystal could induce supersolidity at these apparently too high temperatures.

Acknowledgments

The authors acknowledge partial financial support from the DGI (Spain) Grant No. FIS2008-04403 and Generalitat de Catalunya Grant No. 2009SGR-1003.

-
- [1] Henry R. Glyde, *Excitations in Liquid and Solid Helium* (Clarendon Press, Oxford, UK, 1994).
 - [2] E. Kim and M. H. W. Chan, *Nature* **427**, 225 (2004); *Science* **305**, 1941 (2004).
 - [3] S. Balibar and F. Caupin, *J. Phys.: Condens. Matter* **20**, 173201 (2008).
 - [4] J. Day and J. Beamish, *Nature* **450**, 853 (2007).
 - [5] H.J. Maris and S. Balibar, *J. Low Temp. Phys.* **162**, 12 (2011).

- [6] D. Y. Kim, H. Choi, W. Choi, S. Kwon, E. Kim, and H. C. Kim Phys. Rev. B **83**, 052503 (2011)
- [7] A. Eyal, O. Pelleg, L. Embon, and E. Polturak, Phys. Rev. Lett. **105**, 025301 (2010).
- [8] T. Markovich, E. Polturak, J. Bossy, and E. Farhi, Phys. Rev. Lett. **88**, 195301 (2002).
- [9] N. Gov, Phys. Rev. B **67**, 052301 (2003).
- [10] J. H. Vignos and H. A. Fairbank, Phys. Rev. Lett. **6**, 265 (1961).
- [11] A. F. Schuch and R. L. Mills, Phys. Rev. Lett. **8**, 469 (1962).
- [12] E. R. Grilly and R. L. Mills, Ann. Phys. (N.Y.) **18**, 250 (1962).
- [13] D. O. Edwards and R. C. Pandorf, Phys. Rev. **144**, 143 (1966).
- [14] J. K. Hoffer, W. R. Gardner, C. G. Waterfield, and N. E. Philips, J. Low Temp. Phys. **23**, 63 (1976).
- [15] E. R. Grilly, J. Low Temp. Phys. **11**, 33 (1973).
- [16] F. Pederiva, G. V. Chester, S. Fantoni, and L. Reatto, Phys. Rev. B **56**, 5909 (1997).
- [17] B. Chaudhuri, F. Pederiva, and G. V. Chester, Phys. Rev. B **60**, 3271 (1999).
- [18] D. E. Galli, M. Rossi, and L. Reatto, Phys. Rev. B **71**, 140506(R) (2005).
- [19] D. Ceperley, in *Momentum Distributions*, p. 71, edited by R. N. Silver and P. E. Sokol (Plenum Press, New York, 1989).
- [20] R. C. Blasdell, D. M. Ceperley, and R. O. Simmons, Z. Naturforsch. **48a**, 433 (1993).
- [21] D. M. Ceperley, Rev. Mod. Phys. **67**, 279, (1995).
- [22] K. Sakkos, J. Casulleras, and J. Boronat, J. Chem. Phys. **130**, 204109, (2009).
- [23] M. Takahashi and M. Imada, J. Phys. Soc. Jpn. **53**, 3765, (1984).
- [24] M. Boninsegni, N. V. Prokof'ev, and B. V. Svistunov, Phys. Rev. E **74**, 036701, (2006).
- [25] R. A. Aziz, F. R. W. McCourt, and C. C. K. Wong, Mol. Phys. **61**, 1487 (1987).
- [26] C. Cazorla and J. Boronat, J. Phys.: Condens. Matter **20**, 015223 (2008).
- [27] J. Boronat and J. Casulleras, Phys. Rev. B **49**, 8920 (1994).